High-Fidelity preservation of quantum information during trapped ion transport

Peter Kaufmann, Timm F. Gloger, Delia Kaufmann, Michael Johanning, and Christof Wunderlich*
Department Physik, Naturwissenschaftlich-Technische Fakultät, Universität Siegen, 57068 Siegen, Germany
(Dated: April 10, 2017)

A promising scheme to build scalable quantum simulators and computers is the synthesis of a scalable system using interconnected subsystems. A prerequisite for this approach is the ability to faithfully transfer quantum information between subsystems. With trapped atomic ions this can be realized by transporting ions with quantum information encoded into their internal states. Here, we measure with high precision the fidelity of quantum information encoded into hyperfine states of a $^{171}Yb^+$ ion during ion transport in a micro-structured Paul trap. Ramsey spectroscopy of the ion's internal state is interleaved with up to 4000 transport operations over a distance of $280\,\mu m$ each taking $12.8\,\mu s$. We obtain a state fidelity of $99.9994\,\binom{+6}{-7}\%$ per ion transport.

PACS numbers: 03.67.Lx,37.10.Ty

arXiv:1704.02141v1 [quant-ph] 7 Apr 2017

Ion traps have been a working horse in demonstrating many proof-of-principle experiments in quantum information processing using small ion samples [1]. A major challenge to transform this ansatz into a powerful quantum computing machine that can handle problems beyond the capabilities of classical super computers remains its scalability [2–5]. Error correction schemes allow to fight the ever sooner death of fragile quantum information stored in larger and larger quantum systems, but their economic implementation requires computational building blocks to be executed with sufficient fidelity [6, 7]. Essential computational steps have been demonstrated with fidelities beyond a threshold of 99.99% that is considered as allowing for economic error correction [8], and, thus for fault-tolerant scalable quantum information processing (QIP). These building blocks include single qubit rotation [9, 10], individual addressing of interacting ions [11], and internal state detection [12]. In addition, high fidelity two-qubit quantum gates [10, 13–16] and coherent 3-qubit conditional quantum gates [17, 18] have been implemented.

Straightforward scaling up to an arbitrary size of a single ion trap quantum register, at present, appears unlikely to be successful, because the growing size of a single register usually introduces additional constraints imposed by the confining potential and by the Coulomb interaction of ion strings [19]. Even though, for instance, transverse modes and anharmonic trapping [20] may be employed for conditional quantum logic, a general claim might be, that at some point it is useful to divide a single ion register into subsystems and to exchange quantum information between these subsystems [2–5]. One might do that by transferring quantum information from ions to photons (and vice versa) and by then exchanging photons between subsystems [4, 21].

Alternatively, when exchanging quantum information between spatially separated individual registers within an ion trap-based quantum information processor, the transport of ions carrying this information is an attractive approach [2, 3, 5]. Methods to transport ions in segmented Paul-traps have been developed and demonstrated [22–25], and optimized with respect to the preservation of the motional state during transport [26, 27].

* christof.wunderlich@uni-siegen.de; http://quantenoptik.uni-siegen.de

It is equally important to avoid errors of the quantum information encoded into internal states of ions during transport. Schemes relying on physical transport of ions require shuttling of ions between regions where the actual conditional gates take place (or between memory zones). Canonical schemes for scaling require roughly as many shuttling events as conditional gates [2, 3, 5, 28], and the overall fidelity of gate and shuttling operation is relevant when considering error thresholds. Therefore, in addition to high fidelity of local gates, high fidelity transport is required to not cross a desired error threshold when carrying out single- and multi-qubit quantum gates.

Several experiments have characterized the internal state fidelity $\mathcal{F}$ during transport by measuring the loss of coherence of a superposition state in Ramsey-type measurements. However, the precision reached in these experiments was not yet sufficient to conclude that transport takes place in the fault-tolerant regime required for scaling [22, 24, 26, 27][29]. Here, we demonstrate high fidelity transport of trapped ions over a distance of $280\,\mu m$ with quantum information encoded into internal hyperfine states with a relative error of the qubit states per transport below 10^{-5} which is compatible with fault-tolerant and thus scalable quantum computation.

The determination of $\mathcal{F}$ is limited by the uncertainty of the extracted Ramsey-fringe contrast and the relative error is of the same order as the relative uncertainty of the contrast. In the experiments reported below, we determine the contrast of a Ramsey-type measurement typically with a relative error of $\leq 1 \times 10^{-2}$. Therefore, the straightforward extraction of fringe contrast from experimental data is not sufficient for precise determination of the error taking place during transport. To be able to precisely measure the loss of fidelity, we increase the number of transport operations M. To limit systematic errors due to a possible spatial variation of the qubit coherence time in the trap we design the experiment such, that the ions average position is independent of M for $M > 0$ and compare the contrast after $M = 4000$ with the contrast obtained after $M = 2$ transport operations.

The ion trap is operated with singly charged ^{172}Yb and ^{171}Yb ions. $^{172}Yb^+$ ions possessing no hyperfine structure are employed to determine the efficiency of physical ion transport, while for the analysis of the transport induced decoherence a hyperfine qubit in $^{171}Yb^+$ is used. The ions are Doppler cooled

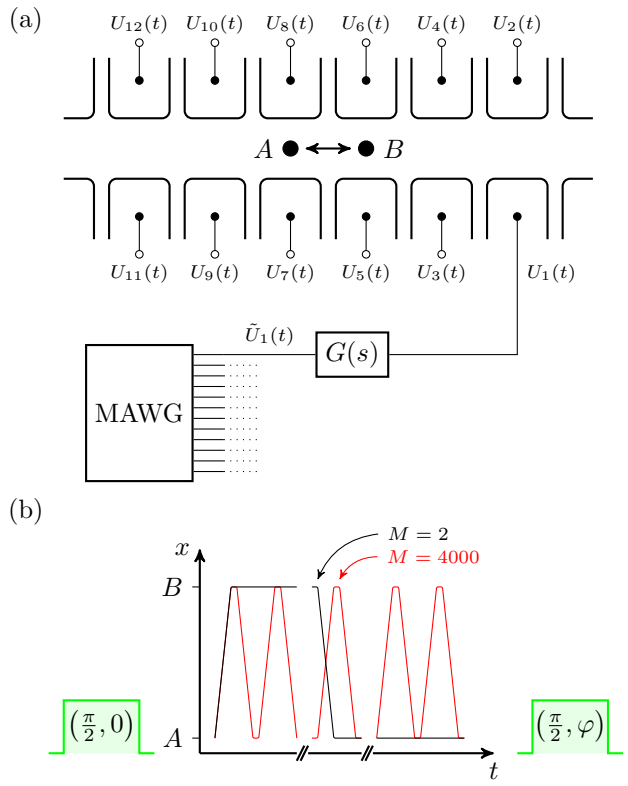

FIG. 1. Schematic of the experiment. *(a)* The voltages $\tilde{U}(t)$ at the multichannel arbitrary waveform generator (MAWG) take the filter characteristic $G(s)$ of the electronics into account to produce suitable voltages $U(t)$ that transports the ion along the x-axis M times between positions A and B. *(b)* The timing of the transport operations is such that the ion is located equally long at A and B. The ion transfer is sandwiched by two $\pi/2$-pulses.

with laser light near 369 nm on the $\left|S_{1/2}\right\rangle - \left|P_{1/2}\right\rangle$ transition. As a qubit we choose the first-order magnetic field insensitive hyperfine qubit composed of the states $|0\rangle \equiv \left|S_{1/2}, F = 0\right\rangle$ and $|1\rangle \equiv \left|S_{1/2}, F = 1, m_F = 0\right\rangle$. The qubit can be efficiently initialized by optical pumping to the $|0\rangle$ state, manipulated coherently by microwave fields and state selective detected by monitoring the resonance fluorescence on the $\left|S_{1/2}, F = 1\right\rangle - \left|P_{1/2}, F = 0\right\rangle$ transition using a EMCCD camera. A detailed description of the laser and microwave setup can be found in [30].

The experiment is carried out in a Paul trap made from a stack of three layers of gold coated alumina wafers [31–33]. The trap is divided into 33 segments, each consisting of two dc-electrodes, and two global rf-electrodes. The voltage applied to each dc-electrode can be controlled individually, while the two rf-electrodes are driven from a single generator. In the experiments reported here, ions were transported by moving the minimum of the trapping potential from the center of one segment A to the center of the next segment B over a distance of $280\,\mu\mathrm{m}$ (see Fig. 1). The required potentials were generated by applying twelve voltage ramps to dc-electrodes in six trap segments of the trap. One additional voltage ramp was applied to a correction electrode to allow for minimization of micromotion perpendicular to the dc-electrodes plane. The dc-voltages are generated using 13 channels of a low noise multi-channel arbitrary waveform generator (MAWG) [34] that is operated with an update frequency of $12.5\,\mathrm{MHz}$.

Methods to transport ions in segmented Paul traps have been investigated elaborately in a number of publications [22–24, 27, 35]. We use the approach worked out in Ref. [36] to calculate an optimized trajectory $\mathbf{r}(t)$ that minimizes ion heating during transport, an implementation of the boundary element method to simulate the potentials generated by our trap geometry [25], and the formalism described in Ref. [35] to calculate suitable transport voltages. We extend and refine this formalism by a method to constructively take into account the characteristics of electronic filters that low-pass our dc electrodes: Instead of trying to compensate the filter behavior after the transport voltage ramps $U(t)$ have been determined, we calculate the accessible voltage range for every point $\mathbf{r}_i = \mathbf{r}(t_i)$ during transport based on the voltage history $U(t_{k<i})$ and limit the potential optimization algorithm to this interval. See Supplemental Material (Section I on page 6) for technical details of the formalism to calculate the transport voltages.

The success of a single transport operation $A \rightarrow B$ or $B \rightarrow A$ is proven by imaging the ion fluorescence for a few milliseconds once the ion is at rest again after having been transported. Because up to 2000 consecutive transport operations $A \rightarrow B \rightarrow A$ are investigated, the success of the overall transport (i.e., during M shuttling events) needs to be shown as well. Imaging the ion for several milliseconds at one position after every second transport operation would add seconds to every single repetition of the experiment, and, more importantly, change the transport dynamics by doppler-cooling of the ions. So to diagnose the success rate of consecutive transfers we implemented an experiment to track the ion during M shuttling operations. During the transport operation the EMCCD camera takes one single image with an exposure time equal to the overall transport duration. Synchronized to the ion transport, we flash the detection laser at position A (B) for $2\,\mu\mathrm{s}$ each time the ion should be at position B (A). The absence of the ion is signified by not detecting scattered resonance fluorescence. This experiment is not exactly tracking the ion but it proves that it is not at a position where it should not be. We also perform measurements that flash the ion at position A (B) when it is expected to be there, but the statistics of these measurements are a factor 15 inferior compared to the more sensitive detection of an absent ion. We drive the $\left|S_{1/2}\right\rangle - \left|P_{1/2}\right\rangle$ dipole transition by a single laser. So the fluorescence rate on this transition is higher for the $^{172}\mathrm{Yb}^+$ isotope without hyperfine and Zeeman splitting compared to the $^{171}\mathrm{Yb}^+$ ion where only a fraction of the 12 possible transitions between $S_{1/2}$ and $P_{1/2}$ are driven in parallel. This experiments is performed using $^{172}\mathrm{Yb}^+$, to profit from the better statistics. We find that $10\,\binom{+12}{-10}$ out of 4000 transport operations are failing, corresponding to a transport fidelity of $99.75\,\%$. See Supplemental Material (Section II on page 7) for a detailed analysis of the shuttling fidelity.

The central goal of the work presented here is to determine the effect of ion transport operations on the qubit's internal

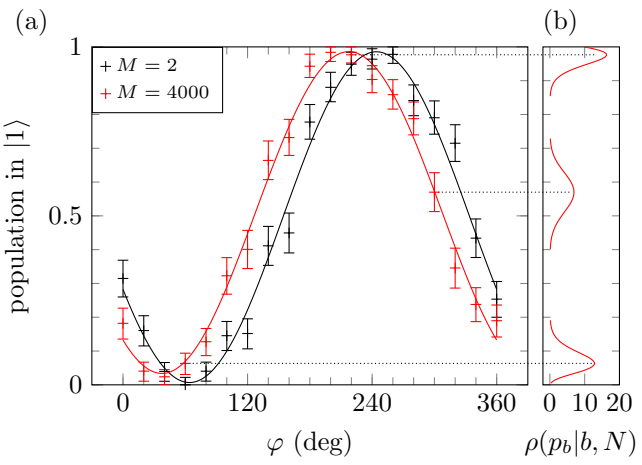

FIG. 2. *(a)* Ramsey fringes for 1 (black) and 4000 (red) ion transport operations. The relative phase φ between the two $\pi/2$-pulses is varied while the time between the pulses is kept constant. The decay of the amplitude due to the additional transport operations is hardly noticeable. *(b)* Three examples for the probability distributions that were used for the likelihood analysis of the data. The probability density $\rho(p_b|b, N)$ for b bright events out of N trials is shown on the horizontal axis as a function of the probability p_b for a projection into the state $|1\rangle$ on the vertical axis.

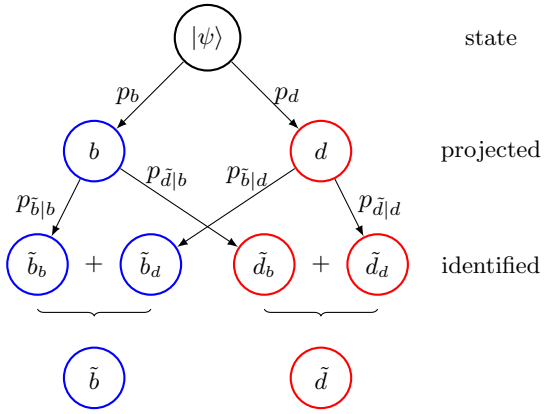

FIG. 3. The likelihood p_b of a state $|\psi\rangle$ to be projected into the bright state is determined by repeating the experiment N times. Out of a total of N measurements, b measurements are projecting the qubit into the bright state, and d measurements are projecting the qubit into the dark state. The qubit states are then identified by analysing the detected resonance fluorescence. Each bright (dark) event is identified correctly with probability $p_{\tilde{b}|b}$ ($p_{\tilde{d}|d}$) and falsely with probability $p_{\tilde{d}|b} = 1 - p_{\tilde{b}|b}$ ($p_{\tilde{b}|d} = 1 - p_{\tilde{d}|d}$). As a consequence the number of identified bright states $\tilde{b} = \tilde{b}_b + \tilde{b}_d$ differs from the true number b of projected states.

state coherence. The internal state coherence is determined by performing a Ramsey-type experiment, where transport operations are executed during the free precession time: We initialize the qubit of a Doppler-cooled ion at position A in the $|0\rangle$ state. Using a microwave $\pi/2$ pulse we prepare the superposition state $|\psi\rangle = 1/\sqrt{2}(|0\rangle - i\,|1\rangle)$. Next the ion is transported M times between the positions A and B. We add waiting times at the positions A and B such, that the total precession time $t_p = 69.44\,\mathrm{ms}$ is independent of M. The waiting time is equally distributed between both positions. After a second $\pi/2$ pulse with a phase φ relative to the first pulse, the qubit state is read out.

We sample the Ramsey interference fringe for $M = 2$ and $M = 4000$ transport operations at 19 phase positions φ. The Ramsey measurement for every setting is repeated 100 times (see Fig. 2).

We monitor fluorescence during Doppler-cooling and use a low fluorescence count (dark or absent ion) as a veto for the last and next Ramsey measurement (about 10 % of the data). Besides electronic readout noise and background counts the detection scheme is limited by off resonant excitation of the transitions $\left|S_{1/2}, F = 0\right\rangle - \left|P_{1/2}, F = 1\right\rangle$ and $\left|S_{1/2}, F = 1\right\rangle - \left|P_{1/2}, F = 1\right\rangle$ and following decay into $\left|S_{1/2}, F = 1\right\rangle$ resp. $\left|S_{1/2}, F = 0\right\rangle$. The former process results in the observation of fluorescence from a qubit originally in the $|0\rangle$ (dark) state, the latter one reduces the fluorescence of the $|1\rangle$ (bright) state. The same effect can be induced by spontaneous decay of the $\left|P_{1/2}, F = 0\right\rangle$ state to the $\left|D_{3/2}, F = 1\right\rangle$ state. By using two separate discrimination thresholds for dark and bright states in the data analysis, we can reduce the probability of wrongly identified states on the cost of reduced statistics [30, 37].

For threshold selection, we add calibration runs to the experiment in which we omit the $\pi/2$-pulses but prepare the ion in the $|0\rangle$ ($|1\rangle$) state before the transport operations, to obtain detection histograms for pure $|0\rangle$ ($|1\rangle$) states. The state $|1\rangle$ is prepared by using a BB1RWR π-pulse [38] that is robust against Rabi frequency errors. The calibration is done separately for both $M = 2$ and $M = 4000$ transport operations in order to account for possible variations of the detection statistics due to transport induced ion heating. Using these calibration measurements we determine threshold values for state discrimination. In addition the probabilities to correctly identify a bright state as bright $p_{\tilde{b}|b}$ and a dark state as dark $p_{\tilde{d}|d}$ can be extracted. We choose thresholds that yield $p_{\tilde{b}|b} = 0.964$ (0.959) and $p_{\tilde{d}|d} = 0.985$ (0.978) for $M = 4000$ ($M = 2$). See Supplemental Material (Section III on page 8) for a more detailed discussion how the thresholds are chosen.

The determination of coherence loss of the qubit state due to the transport operations is done by comparing the amplitudes of the obtained Ramsey fringes for different numbers of transport operations M. As we expect the infidelity to be close to zero we need to employ several statistical methods to get precise results and error estimates. Since the efficiency of state selective detection is below unity, we distinguish between the actual number of projections b and d ($b, d \in \mathbb{N}_0$ and $b + d = N$) into states $|1\rangle$ and $|0\rangle$ and the corresponding numbers $\tilde{b}$ and $\tilde{d}$ identified as $|1\rangle$ and $|0\rangle$ during the data analysis. To reconstruct the true fractional population of the states $|0\rangle$ and $|1\rangle$ of a qubit state $|\Psi\rangle$, we need to infer the numbers b and d from the numbers of identified states $\tilde{b}$ and $\tilde{d}$, as illustrated in Fig. 3. Both, the number of correctly assigned ($\tilde{b}_b$, $\tilde{d}_d$) and falsely assigned states ($\tilde{b}_d$, $\tilde{d}_b$), contribute to $\tilde{b}$ and $\tilde{d}$. By combining the corresponding probabilities, which depend on $p_{\tilde{b}|b}$

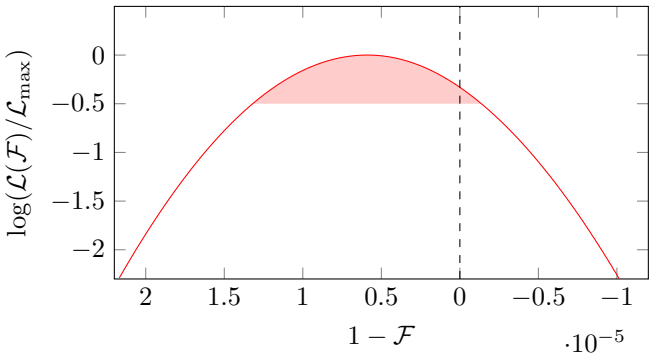

FIG. 4. Likelihood of the internal state fidelity $\mathcal{F}$ during ion transport. The loss of internal state fidelity due to the transfer of the ion is apparent but the case of no loss of coherence is also compatible within the 68% confidence interval (shaded). The log likelihood is calculated by the numerical convolution of the likelihoods $\mathcal{L}_M$.

and $p_{\tilde{d}|d}$, to go from one node in Fig. 3 down to an other one and employing Bayes' theorem one can calculate the probability distribution $\rho(p_b|b,N)$ for the population of a state in $|1\rangle$. Using these results we perform a maximum likelihood analysis and calculate the likelihoods $\mathcal{L}_M(A)$ of the Ramsey fringes amplitudes A for M transport operations. See Supplemental Material (Sections IV and V on pages 8 and 9) for the derivation of $\rho(p_b|b,N)$ and its usage in the likelihood analysis.

Figure 2 (*left*) shows the Ramsey fringes obtained for $M = 2$ and $M = 4000$ transport operations. The error bars indicate the 68 % confidence interval of single data points. The right part displays the probability distribution $\rho(p_b|b,N)$ for three exemplary data points. The amplitude of the $M = 4000$ curve is slightly reduced by 0.013 compared to $M = 2$ and the phases differ by 27°. We measure the magnetic field at 10 positions in the trap by determining the resonance frequency change of the Zeeman qubit encoded in the ground state of $^{171}\mathrm{Yb}^+$ using Ramsey measurements with varying times between $\pi/2$-pulses but fixed phase relations. From these measurements we estimate the gradient of the magnetic field in the direction of the ion transport to be $10.6 \times 10^{-3}\,\mathrm{T/m}$. This gradient results in a 120 Hz difference between the hyperfine splitting of the qubit at positions A and B. From simulations we expect that the mean positions of the ions for 2 and 4000 transfers during the free precession time differ by 0.9 μm, due to non perfect compensation of the dc-electrode filters. This would correspond to a phase difference of 10°.

The state identification probabilities $p_{\tilde{b}|b}$ and $p_{\tilde{d}|d}$ were treated up to this point as fixed errorless parameters. In reality these values are calculated from a finite set of measurements and therefore bear additional uncertainties. We estimate these uncertainties by analyzing the calibration data obtained for state identification using the bootstrapping resampling method [39] and averaging the likelihoods $\mathcal{L}_M(A)$ over the results obtained for different choices of $p_{\tilde{b}|b}$ and $p_{\tilde{d}|d}$. See Supplemental Material (Section VI on page 10) for details of the bootstrap analysis used here.

The likelihood distribution of the internal state fidelity during ion transport (Fig. 4) is calculated by a numerical convolution of the likelihoods of the Ramsey fringe amplitudes A_2 and A_{4000} according to

$$\mathcal{F} = \sqrt[4000-2]{\frac{A_2}{A_{4000}}}\,. \tag{1}$$

We report here a fidelity of the internal qubit state per transport operation of

$$\mathcal{F} = 0.999994\,\left(^{+6}_{-7}\right)\,. \tag{2}$$

This result is obtained under the assumption that each individual transport $A \to B$ and $B \to A$ out of a total of M attempted transports of an ion was actually successful, that is, the transport fidelity was perfect. Taking a finite probability of transport failure into account, the fidelity would change according to $\overline{\mathcal{F}}(M_f) = \mathcal{F}^{\left(\frac{4000-2}{4000-2-M_f}\right)}$, for M_f failing transports. The likelihood of $\mathcal{F}$ is almost gaussian (compare Fig.4), so we expect the error scaling of $\overline{\mathcal{F}}$ to follow $\sigma(\overline{\mathcal{F}}(M_f)) = \frac{4000-2}{4000-2-M_f}\mathcal{F}^{\left(\frac{M_f}{4000-2-M_f}\right)}\sigma(\mathcal{F})$. With the transport fidelity of 99.75 % determined above, a 5σ deviation would result in $M_f = 70$ failed transports. This would reduce the internal state fidelity during ion transport by 1×10^{-7}, which is about an order of magnitude smaller than the statistical uncertainty of $\mathcal{F}$. A systematic error due to imperfect preparation of the states $|0\rangle$ and $|1\rangle$ also do not change the statistical significance of $\mathcal{F}$. See Supplemental Material (Section VII on page 10) for details of the error estimation.

In this work we use the magnetic insensitive hyperfine qubit. Some schemes for QIP with trapped ions using radio-frequency and microwave radiation [40] utilize magnetic field depend states, for example, the qubit composed of $|0\rangle$ and $\left|S_{1/2}, F = 1, m_F = \pm 1\right\rangle$. As the magnetic field sensitive qubit can be recoded into the insensitive qubit and back [18] the results of this paper are also immediately relevant for these QIP schemes.

In summary, we demonstrate by precise measurements and careful data analysis that the physical transport of quantum information encoded in a hyperfine qubit can be carried out with a fidelity better than $1 - 10^{-5}$. This is an important prerequisite, together with high gate fidelities and low cross-talk, for all schemes for scalable QIP with trapped ions that rely on transport of ions.

ACKNOWLEDGMENTS

We acknowledge funding from the European Community's Seventh Framework Programme under Grant Agreement No. 270843 (iQIT), from EMRP (the EMRP is jointly funded by the EMRP participating countries within EURAMET and the European Union).

[1] R. Blatt and D. Wineland, Nature **453**, 1008 (2008).

[2] D. Kielpinski, C. Monroe, and D. J. Wineland, Nature **417**, 709 (2002).

[3] K. M. Svore, A. V. Aho, A. Cross, I. Chuang, and I. L. Markov (IEEE Computer Society, 2006) pp. 58–67.

[4] C. Monroe, R. Raussendorf, A. Ruthven, K. R. Brown, P. Maunz, L.-M. Duan, and J. Kim, Phys. Rev. A **89**, 022317 (2014).

[5] B. Lekitsch, S. Weidt, A. G. Fowler, K. Mølmer, S. J. Devitt, C. Wunderlich, and W. K. Hensinger, Science Advances **3** (2017).

[6] P. W. Shor, Phys. Rev. A **52**, R2493 (1995).

[7] A. Steane, Proceedings: Mathematical, Physical and Engineering Sciences **452**, 2551 (1996).

[8] E. Knill, Nature **463**, 441 (2010).

[9] K. R. Brown, A. C. Wilson, Y. Colombe, C. Ospelkaus, A. M. Meier, E. Knill, D. Leibfried, and D. J. Wineland, Phys. Rev. A **84**, 030303 (2011).

[10] C. J. Ballance, T. P. Harty, N. M. Linke, M. A. Sepiol, and D. M. Lucas, Phys. Rev. Lett. **117**, 060504 (2016).

[11] C. Piltz, T. Sriarunothai, A. F. Varón Rojas, and C. Wunderlich, Nature Communications **5** (2014).

[12] A. H. Burrell, D. J. Szwer, S. C. Webster, and D. M. Lucas, Phys. Rev. A **81**, 040302 (2010).

[13] J. Benhelm, G. Kirchmair, C. F. Roos, and R. Blatt, Nat Phys **4**, 463 (2008).

[14] T. P. Harty, M. A. Sepiol, D. T. C. Allcock, C. J. Ballance, J. E. Tarlton, and D. M. Lucas, Phys. Rev. Lett. **117**, 140501 (2016).

[15] J. P. Gaebler, T. R. Tan, Y. Lin, Y. Wan, R. Bowler, A. C. Keith, S. Glancy, K. Coakley, E. Knill, D. Leibfried, and D. J. Wineland, Phys. Rev. Lett. **117**, 060505 (2016).

[16] S. Weidt, J. Randall, S. C. Webster, K. Lake, A. E. Webb, I. Cohen, T. Navickas, B. Lekitsch, A. Retzker, and W. K. Hensinger, Phys. Rev. Lett. **117**, 220501 (2016).

[17] T. Monz, K. Kim, W. Hänsel, M. Riebe, A. S. Villar, P. Schindler, M. Chwalla, M. Hennrich, and R. Blatt, Phys. Rev. Lett. **102**, 040501 (2009).

[18] C. Piltz, T. Sriarunothai, S. S. Ivanov, S. Wölk, and C. Wunderlich, Science Advances **2** (2016).

[19] M. Johanning, Applied Physics B **122**, 71 (2016).

[20] G.-D. Lin, S.-L. Zhu, R. Islam, K. Kim, M.-S. Chang, S. Korenblit, C. Monroe, and L.-M. Duan, Europhysics Letters **86**, 60004 (2009).

[21] D. Hucul, I. V. Inlek, G. Vittorini, C. Crocker, S. Debnath, S. M. Clark, and C. Monroe, Nat Phys **11**, 37 (2015).

[22] M. A. Rowej, A. Ben-Kish, B. Demarco, D. Leibfried, V. Meyer, J. Beall, J. Britton, J. Hughes, W. M. Itano, B. Jelenković, C. Langer, T. Rosenband, and D. J. Wineland, Quantum Info. Comput. **2**, 257 (2002).

[23] W. K. Hensinger, S. Olmschenk, D. Stick, D. Hucul, M. Yeo, M. Acton, L. Deslauriers, C. Monroe, and J. Rabchuk, Applied Physics Letters **88**, 034101 (2006).

[24] R. B. Blakestad, C. Ospelkaus, A. P. VanDevender, J. M. Amini, J. Britton, D. Leibfried, and D. J. Wineland, Phys. Rev. Lett. **102**, 153002 (2009).

[25] K. Singer, U. Poschinger, M. Murphy, P. Ivanov, F. Ziesel, T. Calarco, and F. Schmidt-Kaler, Rev. Mod. Phys. **82**, 2609 (2010).

[26] R. Bowler, J. Gaebler, Y. Lin, T. R. Tan, D. Hanneke, J. D. Jost, J. P. Home, D. Leibfried, and D. J. Wineland, Phys. Rev. Lett. **109**, 080502 (2012).

[27] A. Walther, F. Ziesel, T. Ruster, S. T. Dawkins, K. Ott, M. Hettrich, K. Singer, F. Schmidt-Kaler, and U. Poschinger, Phys. Rev. Lett. **109**, 080501 (2012).

[28] J. Chiaverini, R. B. Blakestad, J. Britton, J. D. Jost, C. Langer, D. Leibfried, R. Ozeri, and D. J. Wineland, Quantum Information and Computation **5**, 419 (2005).

[29] We assume gaussian errors of the reported Ramsey fringe contrasts and calculate the fidelity as $\mathcal{F} = \sqrt[M]{C_M/C_0})$, where C_0 is the contrast before and C_M after M transport operations.

[30] N. V. Vitanov, T. F. Gloger, P. Kaufmann, D. Kaufmann, T. Collath, M. Tanveer Baig, M. Johanning, and C. Wunderlich, Phys. Rev. A **91**, 033406 (2015).

[31] D. Kaufmann, T. Collath, M. T. Baig, P. Kaufmann, E. Asenwar, M. Johanning, and C. Wunderlich, Applied Physics B **107**, 935 (2012).

[32] S. Schulz, U. Poschinger, K. Singer, and F. Schmidt-Kaler, Fortschritte der Physik **54**, 648 (2006).

[33] S. A. Schulz, U. Poschinger, F. Ziesel, and F. Schmidt-Kaler, New Journal of Physics **10**, 045007 (2008).

[34] M. T. Baig, M. Johanning, A. Wiese, S. Heidbrink, M. Ziolkowski, and C. Wunderlich, Review of Scientific Instruments **84**, 124701 (2013).

[35] R. B. Blakestad, C. Ospelkaus, A. P. VanDevender, J. H. Wesenberg, M. J. Biercuk, D. Leibfried, and D. J. Wineland, Phys. Rev. A **84**, 032314 (2011).

[36] E. Torrontegui, S. Ibáñez, X. Chen, A. Ruschhaupt, D. Guéry-Odelin, and J. G. Muga, Phys. Rev. A **83**, 013415 (2011).

[37] S. Wölk, C. Piltz, T. Sriarunothai, and C. Wunderlich, Journal of Physics B: Atomic, Molecular and Optical Physics **48**, 075101 (2015).

[38] H. K. Cummins, G. Llewellyn, and J. A. Jones, Phys. Rev. A **67**, 042308 (2003).

[39] B. Efron and R. Tibshirani, *An Introduction to the Bootstrap* (Taylor & Francis, 1994).

[40] F. Mintert and C. Wunderlich, Phys. Rev. Lett. **87**, 257904 (2001).

[41] J. Alonso, F. M. Leupold, B. C. Keitch, and J. P. Home, New Journal of Physics **15**, 023001 (2013).

[42] A. V. Oppenheim and R. W. Schafer, *Disrete-Time Signal Processing* (Prentice-Hall, Inc., 1989).

[43] T. F. Gloger, P. Kaufmann, D. Kaufmann, M. T. Baig, T. Collath, M. Johanning, and C. Wunderlich, Phys. Rev. A **92**, 043421 (2015).

Supplemental Material I: Transport potentials

The statistical error of the outcome of our experiment is limited both by the number of transport operations M and the number of repetitions N. As the transport operations are carried out during the free precession time of a Ramsey experiment with limited coherence time, M is directly limited by the transfer time. N is indirectly limited by the overall stability of the experiment apparatus including microwave and laser power stabilities. In order to improve the statistics we implement fast ion transport that includes micromotion minimization and takes electronic filtering into account.

We use the method presented in [36] with the parameters axial trap frequency $\omega_x = 2\pi \times 230\,\mathrm{kHz}$, transfer distance $\Delta x = 280\,\mu\mathrm{m}$, a temporal discretization $\Delta t = (12.5\,\mathrm{MHz})^{-1} = 80\,\mathrm{ns}$ and transport time $T = 160 \cdot \Delta t = 12.8\,\mu\mathrm{s}$ to calculate an ion trajectory $\mathbf{r}_i = \mathbf{r}(t = i \cdot \Delta t)$ discretized in $L = 160$ single steps.

Next a sequence of L potentials is determined with accordingly chosen potential minima and curvatures at the positions $\mathbf{r}_i$. For this we first create a set of basis potentials $\Phi^{(j)}(\mathbf{r})$ of the single electrodes j which are calculated for all electrodes being grounded except electrode j set to a potential U_0 using the boundary element method software package described in [25]. The transport trapping potentials Φ are then obtained as a voltage weighted sum of the individual basis potentials $\Phi^{(j)}$ and the rf-pseudopotenial $\Phi^{(ps)}$ of the rf-electrodes as presented in [35].

For every step i the potentials have to fullfill a couple of boundary conditions. In this experiment the position of the potential minima imposes 3 requirements ($\partial_{x,y,z}\Phi = 0$), the size of the axial trap frequency $\partial_x^2\Phi = m\omega_x^2/q$ and the alignment of the potential axis parallel to the trap's x-axis ($\partial_{xz}^2\Phi = 0$) 2 conditions. We also find it convenient to add a sixth condition $\Phi(\mathbf{r}_i) = \Phi_0$ to define the field at the location $\mathbf{r}_i$ of the potential minimum. These conditions can be expressed as operators $\mathcal{P}$ acting on the potential $\Phi = U^{(j)}\Phi^{(j)} + \Phi^{(ps)}$ and their corresponding eigenvalues. As we use 12 independent controllable dc-electrode potentials the problem is in principle underconstrained.

In practice the limited voltage range and dynamics of any real voltage source narrows down the possible solutions and yields additional constraints. The available minimal and maximal voltages are primary limiting the accessible potential shapes, while the possible dynamics limits the potential changing speed. For the experiment reported here the latter restriction is of primary concern and for simplicity we will not explicitly write down the constraints by maximal voltages in the following formulas.

If the voltage change per discrete time step is limited by δU, the possible voltage U_i for one dc-electrode at step i along the trajectory is limited by

$$U_i \lesseqgtr U_{i-1} \pm \delta U\,. \tag{I1}$$

One can use a constrained optimization algorithm to solve the problem and obtain the voltages $U_i^{(j)}$. If not all boundary conditions can be fullfilled at the same time in the given voltage limits (I1) it can be beneficial to multiply weight factors to the single boundary conditions and prioritize for example a constant trap frequency over the exact position of the potential minimum.

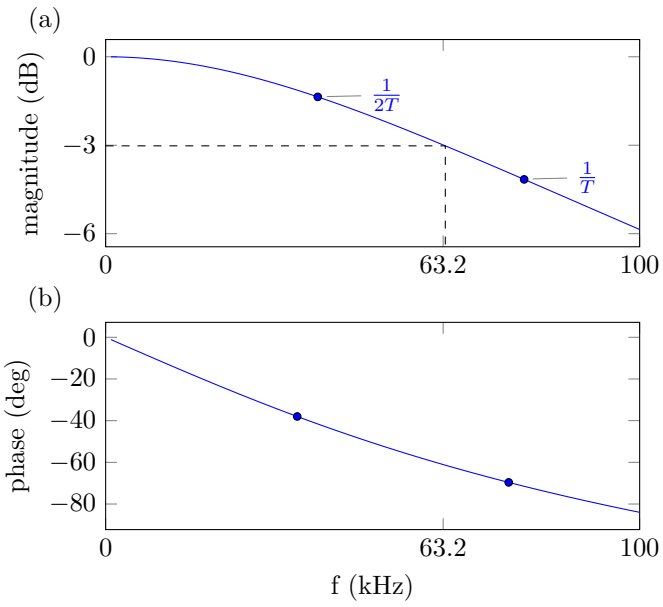

FIG. 5. Bode plot of the electronic filter for a dc-voltage. The inverse transport time $1/T$ is on the order of the cut off frequency of the electronic filters. The horizontal axis of the plot is scaled linear.

1. Modifications for low-pass filter

It is common practice to low-pass the trap's dc-electrodes in order to reduce the electronic noise in the vincinity of the trapped ions. If the dynamics of the transport voltage ramps require frequency components near or even above the cut-off frequency of those filters one needs to distinguish the voltages U at the trap electrodes from the voltages $\tilde{U}$ set at the voltage source.

One possibility to apply fast step function-like potential changes to trap electrodes is the usage of switches located next to the trap that are switching between different voltage channels at a point where the low-pass filtering has already been applied [41].

An other solution is to calculate backwards source voltages $\tilde{U}(t_i)$ such that one gets the desired voltages $U(t_i)$ after the low pass filter. A serious downside of this method is that the maximal possible voltage change δU at the electrodes is not only limited by the maximal possible voltage change $\delta\tilde{U}$ of the source, but is also a function of the history of applied voltages. To ensure realizable voltage sequences one needs to reduce the value of δU in (I1) such that in any case it could be produced by a voltage change of $\delta\tilde{U}$ at the voltage source for all voltage histories. This precaution — if realizable at all — reduces the available dynamics of the voltage source and in consequence the speed of ion transport operations.

We circumvent this problem by incorporating the charac-

teristics of the electronic filters directly in the calculation of the potentials for all steps of the trajectory.

Our electronic filters are constructed by a series of three stages of first order RC low-pass filters and the trap capacitance itself: The first stage terminates our homebuilt programmable voltage source, followed by two stages located next to vacuum interface. Figure 5 shows the corresponding Bode plot. The magnitude of the amplitude in this plot is determined indirectly by measuring the amplitude of a sinus signal parallel to the trap and fitting the capacitances of the trap electrodes. The phase shift is calculated using the obtained model. The cut-off frequency of the system is 63.2 kHz and on the order of the inverse ion transport time $1/T$, showing the necessity to take the filter characteristics into account.

From the electronic circuit we obtain the transfer function $G(s) = \mathcal{L}\{U(t)\}/\mathcal{L}\{\tilde{U}(t)\}$ between source voltage and electrode voltage as quotient of the two-sided Laplace transforms of input and output voltages with the complex parameter $s = i\omega$ [42]. From $G(s)$ a time discrete rational state space transfer function

$$\sum_{n=0}^{n_a} a_n U_{i-n} = \sum_{n=1}^{n_b} b_n \tilde{U}_{i-n} \tag{I2}$$

can be calculated that connects input and output voltages of the electronic filter [42] (b_0 is equal zero such that U_i is independent of $\tilde{U}_i$ — the output is one step behind the input). n_a and n_b are called feedback and feedforward filter orders and are equal 4 in our case. The value of the coefficients a_n and b_n are determined by the resistors and capacitors used.

Solving (I2) for U_i and substituting $\tilde{U}_i = \tilde{U}_{i-1} - \delta\tilde{U}$ resp. $\tilde{U}_i = \tilde{U}_{i-1} + \delta\tilde{U}$ yields the range of the next possible electrode voltages and thus condition (I1) is replaced by:

$$U_i \lessgtr \frac{1}{a_0}\left(b_1(\tilde{U}_{i-1} \pm \delta\tilde{U}) + \sum_{n=2}^{n_b} b_n \tilde{U}_{i-n} - \sum_{n=1}^{n_a} a_n U_{i-n}\right) \tag{I3}$$

2. Micro motion minimization

The trapping potential simulations assume a perfectly fabricated and assembled trap and zero electric stray fields. Deviations from these assumptions require small offset voltages to match the position of the potentials dc- and rf-null. We determine two sets of optimized offset voltages $\Delta U_1^{(j)}$ and $\Delta U_L^{(j)}$ for the start and final position of the ion trajectory using the method described by [43]. For ion positions between these points we are using linearly interpolated values for the offset voltages $\Delta U_i^{(j)}$. The offset voltages are added to the voltages obtained from the potential optimization.

In order to guarantee that the total voltage $\overline{U}_i = U_i + \Delta U_i$ including the offset voltages for micromotion minimization is achievable, the voltage limits (I3) for the potential problem of the ideal trap have to be adjusted by $-\Delta U_i$:

$$U_i \lessgtr \frac{1}{a_0}\left(b_1(\tilde{U}_{i-1} \pm \delta\tilde{U}) + \sum_{n=2}^{n_b} b_n \tilde{U}_{i-n} - \sum_{n=1}^{n_a} a_n U_{i-n} - \Delta U_i\right) \tag{I4}$$

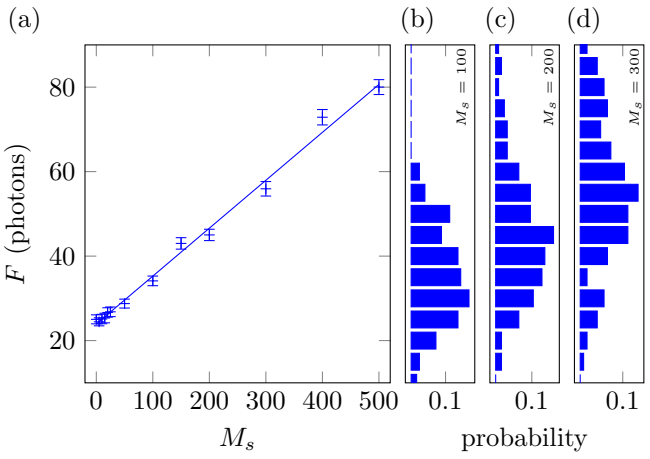

FIG. 6. *(a)* The mean fluorescence F is a linear function of the number M_s of intentionally skipped transport operations. A linear fit yields $0.113(4)$ for the slope and $23.9(6)$ for the offset of the curve. *(b)-(d)* Three sample fluorescence histograms ($M_s = 100, 200, 300$) that were used to extract F. Each histogram holds data of 125 single experiment runs.

The electrostatic problem can now be solved for the electrode voltages U_i and using (I2) suitable source voltages $\tilde{\overline{U}}_{i-1}$ including the filter characteristics and micromotion compensation can be calculated:

$$\tilde{\overline{U}}_{i-1} = \frac{1}{b_1}\left(\sum_{n=0}^{n_a} a_n \overline{U}_{i-n} - \sum_{n=2}^{n_b} b_n \tilde{\overline{U}}_{i-n}\right)$$

The optimization algorithm can be fine tuned by adding several additional constraints to the optimization problem. We limit the voltage difference between voltage source and electrodes by implementing an additional condition $\tilde{\overline{U}} - \overline{U} = 0$ for the potential optimization problem with a small weight. Additionally we favor similar voltages for the transport in both directions ($U^{(j)}_{A\to B}(r_i) - U^{(j)}_{B\to A}(r_i) = 0$) to achieve a closed voltage loop, that is needed for an easy scaling of transport operations. For this condition we use a weight factor that relaxed the condition for coordinates between A and B.

Supplemental Material II: Transport fidelity

To calibrate the measurements of the absent ion we perform the experiment with M_s transport operations $A \to B \to A$ skipped by intent (see Fig. 6). As the ion is detected at

position A when it should have been transported to position B, the detected fluorescence F is increasing with M_s. The expected average photon count F during a experiment of M consecutive transfer operations is given by $F(M_s) = M_s F_b + (M - M_s)F_d$, with F_b and F_d being the average number of photons per detection flash collected from a present (bright) and absent (dark) ion respectively. If a fraction f_s of transport operations $A \rightarrow B$ is failing, $f_s(M - M_s)$ additional bright and $f_s(M - M_s)$ fewer dark events are expected. For the direction $B \rightarrow A$ one has to adjust F by $f_s M_s F_d$ and $-f_s M_s F_b$ accordingly. So the expected total photon number is

$$F(M_s) = F_b[M_s + f_s(M - 2M_s)] + F_d[(M - M_s) - f_s(M - 2M_s)]\,. \qquad \text{(II1)}$$

In an additional run without an ion loaded to the trap we measured the average photon number of an absent ion per flash to be $F_d = 23.5(3)/M$. From a fit of (II1) to the data, we find the probability for transporting the ion as intended per shuttling event to be $1 - f_s = 0.998\,\binom{+2}{-3}$ — corresponding to $10\,\binom{+12}{-10}$ out of 4000 transport operations failing.

Supplemental Material III: Identification probabilities

For the determination of state identification thresholds we incorporate measurements of states prepared in $|0\rangle$ and $|1\rangle$ into the experiment. The probability to identify a bright state as $|1\rangle$ is $p_{\tilde{b}|b} = f_{\tilde{b}|b}/(f_{\tilde{b}|b} + f_{\tilde{d}|b})$, where $f_{\tilde{b}|b}$ is the sum of the probabilities $p^{(b)}(F)$ to measure c_b or more photons F for bright events and $f_{\tilde{d}|b}$ is the summed probability to obtain events with photon numbers less or equal the dark threshold c_d (see Fig. 7 (a). All events $f_{\tilde{s}|b}$ with fluorescence between the two thresholds are excluded in the data analysis. For the identification of dark events one defines $p_{\tilde{d}|d}$, $f_{\tilde{d}|d}$, $f_{\tilde{b}|d}$ and $f_{\tilde{s}|d}$ accordingly. In order to forestall a bias of the identified state the same number of bright and dark events should be excluded from the data analysis. With the cumulative distribution functions $f^{(b)}(c) = \sum_{F \le c} p^{(b)}(F)$ and $\overline{f}^{(d)}(c) = 1 - \sum_{F \le t} p^{(d)}(F)$ one finds

$$f_{\tilde{s}|b} = f^{(b)}(c_b - 1) - f^{(b)}(c_d)$$

and

$$f_{\tilde{s}|d} = \overline{f}^{(d)}(c_b - 1) - \overline{f}^{(d)}(c_d)\,.$$

From the constraint $f_{\tilde{s}|b} = f_{\tilde{s}|d}$ the condition

$$f^{(b)}(c_b - 1) + \overline{f}^{(d)}(c_b - 1) = f^{(d)}(c_d) - f^{(b)}(c_d)$$

follows. In Fig. 7 (c) the selection of a pair of matched thresholds c_b, c_d for $M = 4000$ is illustrated. The events in the gray shaded area (6 %) are excluded from the further data analysis, yielding identification probabilities $p_{\tilde{b}|b} = 0.964$ and $p_{\tilde{d}|d} = 0.985$.

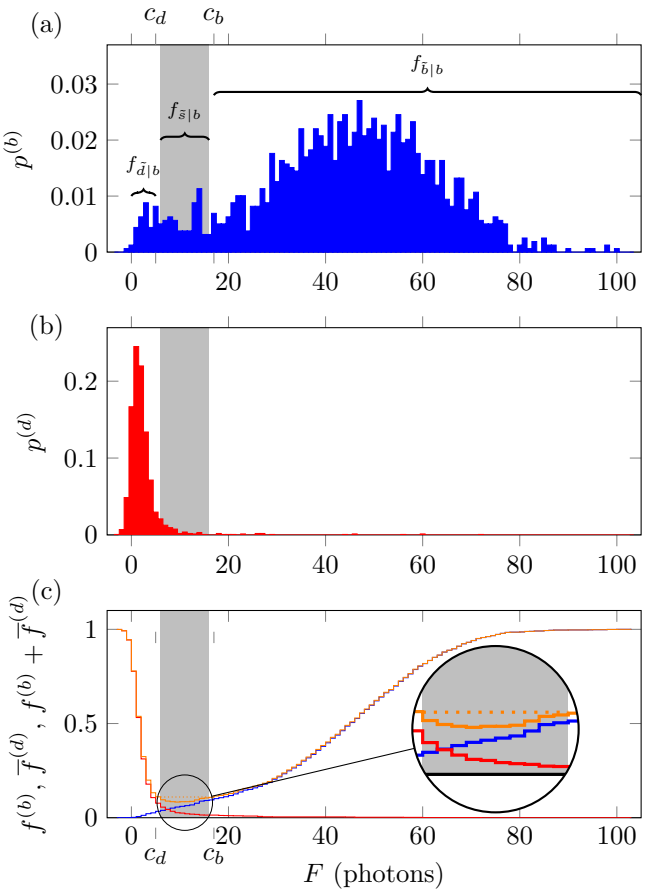

FIG. 7. Histograms of the detected fluorescence of an ion prepared in the internal state $|1\rangle$ *(a)* and $|0\rangle$ *(b)* after $M = 4000$ transport operations. To improve the state detection we use two thresholds for state discrimination and drop all ambiguous events in between (gray shaded area). The probability to correctly identify $|1\rangle$ is $p_{\tilde{b}|b} = f_{\tilde{b}|b}/(f_{\tilde{b}|b} + f_{\tilde{d}|b})$. Figure *(c)* illustrates how appropriate thresholds can be determined by using the sum (orange) of the cumulative distribution functions (see Appendix III).

Supplemental Material IV: State population reconstruction

A single measurement projects the state $|\psi\rangle = \alpha\,|0\rangle + \beta\,|1\rangle$ with the probabilities $p_d = |\alpha|^2$ and $p_b = |\beta|^2$ to the dark and bright state. N repetitions of the measurement produce d dark and b bright states, respectively. One needs to distinguish the true number of bright states b from the number $\tilde{b}$ of states that are identified as bright in the data analysis.

In the following the probability of projecting b times to the bright state is deduced from $\tilde{b}$ and the state probability density function of p_b from b (going upwards in main text Fig. 3). By combining these results the state population density function $\rho(p_b|\tilde{b}, N)$ as a function of identified states and number of measurements N is obtained.

a. identified state → projected state The number $\tilde{b}$ is the sum of the events $\tilde{b}_b$ where bright states are correctly identified as bright (probability $p_{\tilde{b}|b}$) and the events $\tilde{b}_d$ where dark states are wrongly identified as bright (probability $p_{\tilde{b}|d}$). The prob-

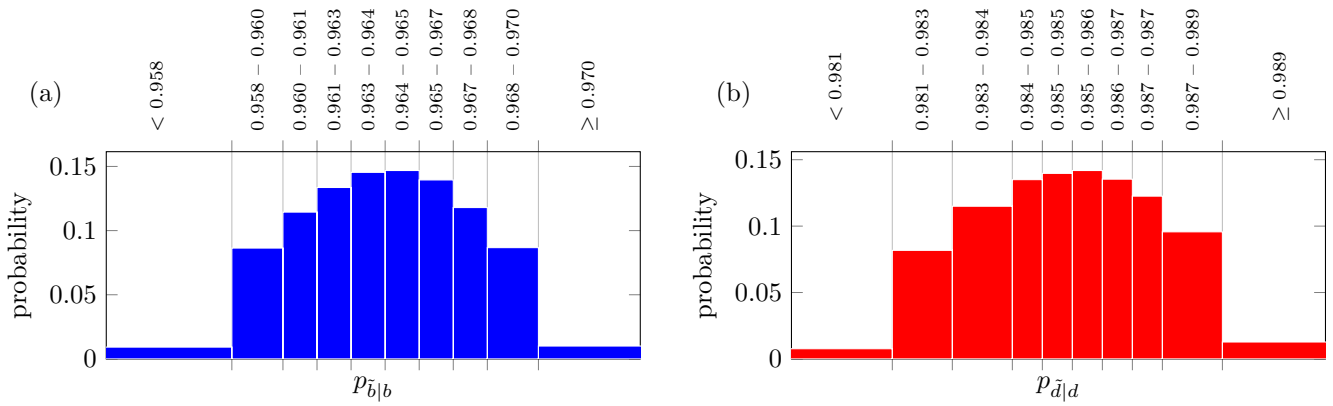

FIG. 8. State detection fidelities for $M = 4000$ transport operations. The histograms are generated by repeatedly selecting random sets from the calibration measurements. The bin edges are selected such that the number of total events in the single bins are closely matching while avoiding binning effects at the same time. The first and last intervals are only shown in part.

abilities to correctly identify $\tilde{b}_b$ events out of b bright states $P(\tilde{b}_b|b)$ and falsely identify $\tilde{b}_d$ events out of d dark states $P(\tilde{b}_d|d)$ are binomially distributed:

$$P(\tilde{b}_b|b) = \binom{b}{\tilde{b}_b} (p_{\tilde{b}|b})^{\tilde{b}_b} (1 - p_{\tilde{b}|b})^{b-\tilde{b}_b} \tag{IV1}$$

$$P(\tilde{b}_d|d) = \binom{d}{\tilde{b}_d} (p_{\tilde{b}|d})^{\tilde{b}_d} (1 - p_{\tilde{b}|d})^{d-\tilde{b}_d} \tag{IV2}$$

So the probability to identify $\tilde{b}$ states as bright from N measurements and b bright states $P(\tilde{b}|b, N)$ can be expressed as the sum of the probabilities (IV1) and (IV2) over all possible compositions of $\tilde{b} = \tilde{b}_b + \tilde{b}_d$

$$P(\tilde{b}|b, N) = \sum_{\tilde{b}_b=0}^{\tilde{b}} P(\tilde{b}_b|b) P(\underbrace{\tilde{b} - \tilde{b}_b}_{\tilde{b}_d} | \underbrace{N - b}_{d}) . \tag{IV3}$$

Then the probability $P(b|\tilde{b}, N)$ of b projections to the bright qubit state in an experiment where $\tilde{b}$ out of N measurements were identified as bright can be calculated using Bayes' theorem:

$$P(b|\tilde{b}, N) = \frac{P(\tilde{b}|b, N) P(b|N)}{P(\tilde{b}|N)} \tag{IV4}$$

Every measurement outcome is a priori same likely and the total probability normalized to 1. So $P(b|N) = 1/(N + 1)$ follows and the probability $P(\tilde{b}|N)$ can be written as the sum $P(\tilde{b}|N) = \sum_{b=0}^{N} P(\tilde{b}|b, N) P(b|N)$. Utilizing this in (IV4) yields:

$$P(b|\tilde{b}, N) = \frac{P(\tilde{b}|b, N)}{\sum_{b'=0}^{N} P(\tilde{b}|b', N)} \tag{IV5}$$

b. projected state → state population The probability $P(b|p_b, N)$ to obtain b bright events for p_b and N given, is distributed binomially. For the data analysis the inverse information, the distribution of p_b for a given experimental result b, is relevant. With Bayes' theorem

$$\rho(p_b|b, N) = P(b|p_b, N) \frac{\rho(p_b)}{P(b|N)} \tag{IV6}$$

follows. By using again the fact that every measurement outcome is a priori same likely ($\rho(p_b) = 1$) one finds from (IV6), that the distribution of p_b is

$$\rho(p_b|b, N) = (N + 1) \binom{N}{b} (p_b)^b (1 - p_b)^{N-b} .$$

With $\mathrm{B}(b + 1, N - b + 1)^{-1} = \left[(N + 1)\binom{N}{b}\right]^{-1}$, where $\mathrm{B}(b + 1, N - b + 1) = \int_0^1 p^b (1 - p)^{N-b} dp$ denotes the beta function, it follows that p_b is subject to the beta probability density function

$$\rho(p_b|b, N) = \frac{(p_b)^b (1 - p_b)^{N-b}}{\mathrm{B}(b + 1, N - b + 1)} \tag{IV7}$$

for a given measurement result $(b, d) = (b, N - b)$.

c. identified state → state population The final step to reconstruct the state populations is to obtain the probability density function $\rho(p_b|\tilde{b}, N)$ of p_b for an experiment where $\tilde{b}$ results out of N were identified as bright. This is done by summing up (IV7) over all b weighted by the respective probabilities $P(b|\tilde{b}, N)$ (IV5):

$$\rho(p_b|\tilde{b}, N) = \sum_{b=0}^{N} \rho(p_b|b, N) P(b|\tilde{b}, N) \tag{IV8}$$

Supplemental Material V: Likelihood analysis

As a measure for the loss of qubit state fidelity due to ion transport we are using the decay of the contrast of Ramsey fringes. The state population varies as a function of the relative phase of the second $\pi/2$-pulse and can be parameterized by

$$p_b(\varphi) = B + A \sin(\varphi - \Phi) \tag{V1}$$

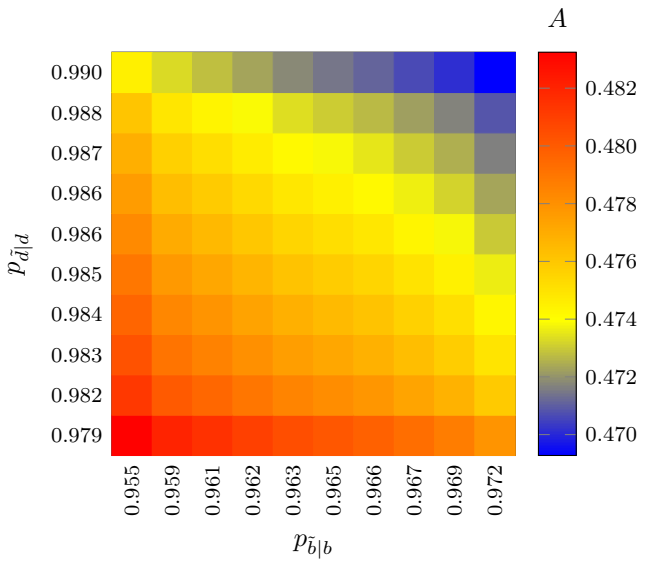

FIG. 9. The amplitude A of the fitted Ramsey fringes depends on the assumed state identification probabilities $p_{\tilde{b}|b}$ and $p_{\tilde{d}|d}$. If the states can be identified with lower probability the likelihood analysis scales the measurement data accordingly towards the extreme values 0 and 1 resulting in a higher amplitude. To account for this effect the data analysis is carried out for 100 combinations of $p_{\tilde{b}|b}$ and $p_{\tilde{d}|d}$ with similar likelihoods.

with the amplitude A, offset B and phase shift Φ. We fit the model for both number of transfer operations M by maximizing the log likelihood

$$\log \mathcal{L}(A, B, \Phi)_M = \sum_{k=1}^{K} \log \rho(B + A \sin(\varphi_k - \Phi) | \tilde{b_k}, N_k) \tag{V2}$$

using the probability density function (IV8) for the K data points $(\tilde{b_k}, N_k)$.

Supplemental Material VI: Bootstrap analysis of the calibration data

The state identification probabilities $p_{\tilde{b}|b}$ and $p_{\tilde{d}|d}$ are a parameter of the data analysis. We estimate there uncertainties by applying the bootstrapping resampling method [39] to the calibration data. Figure 8 shows the distributions of $p_{\tilde{b}|b}$ and $p_{\tilde{d}|d}$ obtained from 10000 resampling runs. Binning of the data is done such that every of the 10 bins represents almost the same fraction $w(p_{\tilde{b}|b})$ ($w(p_{\tilde{d}|d})$) of results. So every combination of $p_{\tilde{b}|b}$ and $p_{\tilde{d}|d}$ has almost the same significance of $w(p_{\tilde{b}|b}, p_{\tilde{d}|d}) = w(p_{\tilde{b}|b}) w(p_{\tilde{d}|d}) \approx 1/100$.

The maximum likelihood fit of the Ramsey fringes is carried out for every such combination using the weighted mean value for $p_{\tilde{b}|b}$ and $p_{\tilde{d}|d}$ in the corresponding interval and the resulting profile likelihood function $\mathcal{L}_M(A|p_{\tilde{b}|b}, p_{\tilde{d}|d})$ of the parameter A is calculated. Figure 9 shows the most likely amplitudes for each combination of the state identification probabilities. If one assumes smaller state identification probabilities the amplitude is generally assumed to be higher.

Figure 10 shows the log likelihood function $\mathcal{L}_M(A)$ obtained by summing up the single likelihoods

$$\mathcal{L}_M(A) = \sum_{p_{\tilde{b}|b}, p_{\tilde{d}|d}} w(p_{\tilde{b}|b}, p_{\tilde{d}|d}) \mathcal{L}_M(A|p_{\tilde{b}|b}, p_{\tilde{d}|d}) \tag{VI1}$$

Again one can see that the most likely amplitude of the Ramsey fringes for more transport operations is slightly smaller. The 1σ confidence interval of the amplitude for $M = 2$ and $M = 4000$ are overlapping. By comparing the likelihoods obtained with and without usage of the bootstrapped distributions $p_{\tilde{b}|b}$ and $p_{\tilde{d}|d}$ one can see that the inclusion of this statistical error source is broadening and slightly shifting the maximum of the calculated likelihoods.

Supplemental Material VII: Preparation errors

The identification probabilities are determined under the assumption that the bright and dark states could be prepared with high fidelity. We assume a preparation fidelity of $\mathcal{F}_{prep.} > 1 - 1 \times 10^{-4}$ and a fidelity of the fault tolerant BB1RWR π-pulse of $\mathcal{F}_{\pi} > 1 - 1.3 \times 10^{-4}$. The corresponding maximal bias of the identification probabilities are -9.5×10^{-5} ($p_{\tilde{b}|b}$) and -2.2×10^{-4} ($p_{\tilde{d}|d}$). A data analysis assuming these biases yields insignificant changes to the overall result for the internal state fidelity during ion transport.

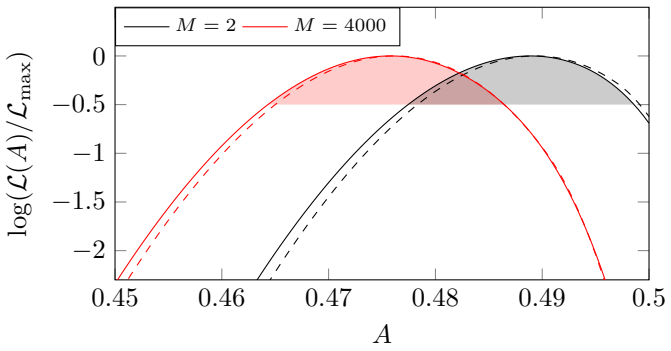

FIG. 10. Log likelihoods for the amplitude of the Ramsey fringes with 2 and 4000 transfer operations. The 68% confidence intervals (shaded) are overlapping. The log likelihoods are calculated by adding up the likelihoods $\mathcal{L}_M(A|p_{\tilde{b}|b}, p_{\tilde{d}|d})$ obtained by data analysis for different pairs of $p_{\tilde{b}|b}$ and $p_{\tilde{d}|d}$. For comparision the dashed curves are showing one pair of likelihoods $\mathcal{L}_M(A|p_{bb}, p_{dd})$ that are determined from the Ramsey fringes in main text, Fig. 2.